Article

Physically-Based Retrieval of Canopy Equivalent Water Thickness Using Hyperspectral Data

Matthias Wocher * , **Katja Berger** , **Martin Danner** , **Wolfram Mauser and Tobias Hank**

Department of Geography, Ludwig-Maximilians-University Munich, Luisenstraße 37, 80333 Munich, Germany; katja.berger@lmu.de (K.B.); martin.danner@iggf.geo.uni-muenchen.de (M.D.); w.mauser@lmu.de (W.M.); tobias.hank@lmu.de (T.H.)
* Correspondence: m.wocher@lmu.de; Tel.: +49-892-180-6695

check for updates

Abstract: Quantitative equivalent water thickness on canopy level (EWT_{canopy}) is an important land surface variable and retrieving EWT_{canopy} from remote sensing has been targeted by many studies. However, the effect of radiative penetration into the canopy has not been fully understood. Therefore, in this study the Beer-Lambert law is applied to inversely determine water content information in the 930 to 1060 nm range of canopy reflectance from measured winter wheat and corn spectra collected in 2015, 2017, and 2018. The spectral model was calibrated using a look-up-table (LUT) of 50,000 PROSPECT spectra. Internal model validation was performed using two leaf optical properties datasets (LOPEX93 and ANGERS). Destructive in-situ measurements of water content were collected separately for leaves, stalks, and fruits. Correlation between measured and modelled water content was most promising for leaves and ears in case of wheat, reaching coefficients of determination (R^2) up to 0.72 and relative RMSE (rRMSE) of 26% and in case of corn for the leaf fraction only ($R^2 = 0.86$, rRMSE = 23%). These findings indicate that, depending on the crop type and its structure, different parts of the canopy are observed by optical sensors. The results from the Munich-North-Isar test sites indicated that plant compartment specific EWT_{canopy} allows us to deduce more information about the physical meaning of model results than from equivalent water thickness on leaf level (EWT) which is upscaled to canopy water content (CWC) by multiplication of the leaf area index (LAI). Therefore, it is suggested to collect EWT_{canopy} data and corresponding reflectance for different crop types over the entire growing cycle. Nevertheless, the calibrated model proved to be transferable in time and space and thus can be applied for fast and effective retrieval of EWT_{canopy} in the scope of future hyperspectral satellite missions.

Keywords: hyperspectral; spectroscopy; equivalent water thickness; canopy water content; agriculture; EnMAP

1. Introduction

The quantification of water stored in agricultural plants plays an essential role in understanding the impact of cultivated areas on the earth's water cycle. Due to its close association to biochemical factors, such as vegetation transpiration [1] and net primary production [2], the knowledge of quantities of water contained within agricultural crops is crucial, particularly for the development of environmental process models [3,4]. Moreover, quantifying canopy water content is important in regards to the water use efficiency of plants [5], evaluation of plant physiological status and health [6,7], and crop ripening monitoring [8].

Within the optical spectral domain (400 nm–2500 nm), absorption by vegetation liquid water occurs in the near-infrared (NIR) at 970 nm and 1200 nm and in the shortwave infrared (SWIR) at 1450 nm and 1950 nm [9,10]. Due to a higher absorption coefficient in the SWIR [11] most of the

early studies combined those wavelengths with water insensitive wavelengths in the NIR to define empirical narrow-band indices for water content retrieval [12–15]. However, the strong absorption by water may saturate those bands at high water contents in optically thick canopies [16]. Moreover, absorption by atmospheric water vapor at 1450 nm and 1900 nm results in noisy measurements which renders these spectral regions unsuitable for further analysis [9], both for top-of-atmosphere (TOA) and top-of-canopy (TOC) spectroscopy. Some vegetation biophysical variables may disturb the signal of water: for instance Jacquemoud, et al. [17] noted that the leaf area index (LAI) masks the water signal between 1000 nm and 1400 nm and advised caution when using such indices for water retrieval. The comparatively low 970 nm water absorption depth is embedded in an area of generally high vegetation reflectance in the NIR. Due to low absorption it is expected that radiation at 970 nm penetrates deeper into the canopy reflecting a larger portion of its total water content without a tendency to saturation [18–22]. Therefore, Peñuelas, et al. [6,7] developed the 970 nm water index (WI) to retrieve relative plant water concentration (PWC). In the following, other studies also focused on the 970 nm absorption to estimate canopy water content [3,5,23,24].

Methodologically, the definition of a narrow-band spectral index to retrieve vegetation water content information constitutes the parametric regression type of methods. Their simplicity and thus computational feasibility make them highly desirable for large-scale remote sensing applications. However, a fundamental problem of parametric regression methods is their lack of generality and transferability [25]. Since indices are not solely influenced by liquid water, but also affected by leaf internal structure and leaf dry matter [26] or canopy structure, LAI and soil background [15,27,28], the established regression-based relationships and estimated quantities of water stored in a canopy are limited to local conditions [29]. Accordingly, the obtained results are site-, time- and crop-specific [30]. Moreover, as more hyperspectral image data with a continuous spectral coverage become accessible, the limited use of a small number of bands does not correspond to the up to date possibilities in view of the available data information density.

For the implications given, physically based model inversion methods have been introduced as a promising alternative to retrieve biochemical and biophysical vegetation variables. Radiative transfer models (RTM) describe interactions between solar radiation and vegetation constituents using physical laws. Their ability to generate an infinite number of simulated spectra with known input parameters conversely allows their inversion in order to estimate the underlying parameters. For the inversion of RTMs, a variety of strategies have been applied. These include numerical optimization algorithms, look-up table (LUT) approaches, artificial neural networks (ANN) and other machine learning algorithms (for an overview please refer to Verrelst, et al. [25,31]). Although RTM-based inversion methods are considered to be physically sound, the techniques require profound knowledge, are often computationally demanding and are mathematically highly non-linear [31,32]. Another limitation of RTM-inversion is the ill-posed nature or equifinality of model inversion. Many different parameter sets may be equally valid in terms of their ability to reproduce a measured reflectance spectrum (for a discussion of this topic see Atzberger and Richter [33]).

In view of future hyperspectral satellite missions like Italian PRISMA [34], US HyspIRI [35], Israeli-Italian SHALOM [36], European CHIME [37], and German EnMAP [38] fast and efficient retrieval methods for large datasets are required. Mathematically simpler physically-based approaches have been applied before to circumvent the equifinality problem and to reduce the computational effort of RTM-based model inversion. Green, et al. [39,40] originally incorporated the Beer-Lambert law to separate liquid water from atmospheric water vapor and determine both to allow the retrieval of surface reflectance from measured AVIRIS radiance. Thereby, the Beer-Lambert law was applied to directly infer the path length through optically active liquid water, i.e., the equivalent water thickness (EWT), from a measured reflectance spectrum using water absorption coefficients for pure liquid water [41,42]. Since multiple NIR scattering, and the attendant increase in optical path length at both the leaf and the canopy scale are not accounted for in the simple Beer-Lambert law [43,44], absolute quantification of EWT can only be achieved by calibration. Subsequently, validation has to

be performed on accurate in-situ measurements. Studies that aimed at separating all three phases of water were not designed to quantify canopy water content in absolute terms and therefore accurate measurements were not carried out [45–48]. On the other hand, studies which derived water content explicitly by applying the Beer-Lambert law often relied on the assumption that upscaling leaf EWT to canopy water content (CWC) could be done by a simple multiplication with the leaf area index (LAI) (see references [5,23,25,49,50]). In other publications, biomass sampling strategies have not been designed to deduce the single water components of a canopy that an optical sensor can actually detect (e.g., references [21,51–53]). Consequently, validation of these approaches could not approve translation into transferable and generally applicable retrieval tools [42].

Therefore, the objective of the present study was to test the performance of the Beer-Lambert law to retrieve crop water content from spectra with a contiguous spectral coverage around 970 nm and perform validation separately for leaves, stalks, and fruits by means of the two very different crop types: corn and winter wheat.

2. Materials

2.1. Munich-North-Isar Test Site

2.1.1. Biomass Sampling and Water Content Determination

Biomass collection was performed in 2015, 2017, and 2018 at three winter wheat fields (*triticum aestivum*) and two corn fields (*zea mays*) of communal farmland 30 km north of Munich (southern Germany) east of the river Isar (Table 1, Figure 1).

Figure 1. Munich-North-Isar test sites overview (**left**) and exemplary 2017 simulated 30 × 30 m corn EnMap-pixel with 9 ESUs (**right**).

Table 1. Munich-North-Isar winter wheat and corn test sites, locations, periods of sample collection, number of biomass samples, and number of spectral measurements at cloud-free days.

Crop Type	Coordinates	Sampling Period	No. of Samplings	No. of Spectral Measurements
Winter wheat	48°14′51.46″N 11°42′24.10″E	10 April–29 July 2015	17	7
Winter wheat	48°14′56.70″N 11°43′03.60″E	29 March–17 July 2017	16	12
Winter wheat	48°14′52.27″N 11°42′57.06″E	04 April–13 July 2018	12	7
Corn	48°17′06.56″N 11°42′49.98″E	8 June–15 September 2017	11	8
Corn	48°14′56.70″N 11°43′03.60″E	25 May–29 August 2018	13	6

Within the fields, three different sampling points were selected based on long-term biomass distribution pattern observations (TalkingFields Base Map: www.talkingfields.de) representing low, medium, and high persistent relative fertility.

Plant leaf water content is commonly expressed as equivalent water thickness (EWT, Equation (1)) corresponding to a hypothetical thickness of a single layer of water averaged over the whole leaf area [10]:

$$\text{EWT} = \frac{\text{FW} - \text{DW}}{\text{A}} \left[\text{g cm}^{-2}\right] \text{ or } [\text{cm}], \quad \left[\text{kg m}^{-2}\right] \text{ or } [\text{mm}] \tag{1}$$

where FW is the fresh sample weight, DW is the oven dry weight and A is the leaf area. While EWT refers to the water content on leaf level, canopy water content (CWC, Equation (2)) is commonly derived through extrapolation by means of the LAI:

$$\text{CWC} = \text{EWT} * \text{LAI} \tag{2}$$

Due to the linkage of LAI to the whole canopy, CWC may be biased towards the leaf fraction. Furthermore, CWC does not allow inferring the actual water detectability of plant components in a canopy from total detected water. Consequently, in this study total $\text{EWT}_{\text{canopy}}$ (EWT_{leaf} + $\text{EWT}_{\text{stalk}}$ + $\text{EWT}_{\text{fruit}}$) will be defined as the above-ground total equivalent water layer averaged over one square meter of ground surface (Equation (3)).

$$\text{total EWT}_{\text{canopy}} = \sum (\text{FW}_{\text{leaves+stalks+fruits}} - \text{DW}_{\text{leaves+stalks+fruits}}) * \text{A}_{\text{g}}^{-1} \tag{3}$$

where A_{g} denotes the ground area. To monitor the development of total amounts of water stored in the canopy throughout the growing season, biomass samples were collected on a weekly basis. In case of wheat, a minimum transect of 50 cm along a sowing track or an area of 0.25 m^2 was cut at soil level. For corn, 2–3 plants were cut. In-field plant density was obtained by counting plants and rows per meter. The samples were separated into leaf, stalk and fruit compartments, weighed in fresh state and oven-dried until constant weight for 24 h at 105 °C before dry weight was determined. EWT_{leaf}, $\text{EWT}_{\text{stalk}}$, $\text{EWT}_{\text{fruit}}$ (EWT_{ear} and EWT_{cob}, respectively) and total $\text{EWT}_{\text{canopy}}$ per cm^2 (Table 2) were calculated from laboratory results (specific water contents per ground area) and from farm management metadata (plants per meter and row spacing). The phenology was determined according to secondary growth stages of the BBCH-scale [54].

Table 2. Statistics (range, mean, standard deviation) for in-situ measured EWT_{leaf}, $\text{EWT}_{\text{stalk}}$, $\text{EWT}_{\text{fruit}}$, total $\text{EWT}_{\text{canopy}}$ and BBCH-range. Values correspond to measurements with available spectral reflectance data.

Year	2015	2017		2018	
Crop Type	**Winter Wheat**	**Winter Wheat**	**Corn**	**Winter Wheat**	**Corn**
BBCH range [-]	22–87	25–87	30–85	28–87	32–83
EWT_{leaf}: range [cm]	0.007–0.179	0.005–0.182	0.009–0.104	0.045–0.121	0.095–0.161
mean (std) [cm]	0.066 (0.058)	0.082 (0.050)	0.059 (0.035)	0.082 (0.027)	0.132 (0.023)
$\text{EWT}_{\text{stalk}}$: range [cm]	0.012–0.256	0.003–0.275	0.008–0.295	0.019–0.268	0.252–0.619
mean (std) [cm]	0.123 (0.084)	0.144 (0.089)	0.161 (0.115)	0.126 (0.099)	0.472 (0.126)
$\text{EWT}_{\text{fruit}}$: range [cm]	0.000–0.100	0.000–0.112	0.000–0.248	0.000–0.148	0.000–0.306
mean (std) [cm]	0.044 (0.045)	0.045 (0.045)	0.068 (0.100)	0.048 (0.068)	0.171 (0.123)
Total $\text{EWT}_{\text{canopy}}$: range [cm]	0.041–0.417	0.019–0.490	0.017–0.606	0.064–0.503	0.347–1.019
mean (std) [cm]	0.233 (0.141)	0.271 (0.145)	0.289 (0.221)	0.256 (0.170)	0.775 (0.227)

2.1.2. Spectroscopic Measurements

At each study site, a 30 × 30 m grid of nine 10 × 10 m squares was marked out delineating the elementary sampling units (ESU). This grid layout was designed to trace the geometric properties of one EnMAP pixel; hence, regarding the viewing geometry and grid location, the sensors descending orbit and inclination angle of 97.96° was accounted for (Table 1). At each sampling date with clear

sky conditions (Table 1) all nine ESUs were revisited and spectral measurements were taken using an Analytical Spectral Devices Inc. (ASD, Boulder, CO, USA) FieldSpec3 Jr. spectroradiometer with an effective spectral resolution of 3 nm in the VIS ($\leq$700 nm) and 10 nm in the NIR and SWIR ($\leq$2500 nm). Five nadir measurements were conducted per ESU at a height of 25 cm above the canopy, the same height at which the white reference panel (OptoPolymer, Munich, Germany) could be fully observed with the instruments field of view of 25°. Throughout the measurements, the sensor was slightly moved back and forth manually while maintaining the observation angle to obtain a representative spectral sample of the canopy. The five recorded spectra were averaged per ESU and a spatial mean of the nine ESUs was calculated to provide reflectance of the complete 30 × 30 m grid. Further, post-processing included splice-correction, white reference baseline calibration, and slight smoothing using a Savitzky-Golay-Filter with a frame size of 13 nm.

Note that it was not possible to conduct destructive sampling at exactly the same locations where the continuous spectral measurements were taken. However, due to averaging of spectral sampling points over the 30 × 30 m sampling area, it was possible to capture the in-field variability and therefore to represent average field water conditions.

Altogether, the collected dataset comprised destructively measured, plant compartment specific water content samples with corresponding spectral measurements at 26 dates for wheat and 14 dates for corn over three and two years, respectively (see Tables 1 and 2).

2.2. Leaf Optical Data

Preliminary tests of the EWT_{canopy} retrieval model presented in this study were performed on two different leaf optical datasets. The LOPEX93 database was established in 1993 by the Joint Research Centre (JRC, Ispra, Italy). It associates transmittance and reflectance in the range of 400–2500 nm with biophysical and biochemical measurements of 66 leaf samples from 45 species [55]. In total, the database comprises 330 spectra with corresponding measurements of EWT. Secondly, tests were performed on the ANGERS database containing 276 reflectance spectra and EWT measurements of 43 species [56]. While woody species make up the majority of the ANGERS database, both datasets represent a large variety of leaf internal structure and spectra.

2.3. Radiative Transfer Models and Look-Up Tables

To check consistency between leaf optical data and modelled spectra, large look-up tables (LUT) using the RTMs PROSPECT and PROSAIL were created. PROSAIL [17] is coupling the *Leaf Optical Properties Spectra* model PROSPECT [57] and the turbid medium canopy reflectance model 4SAIL (*Scattering by Arbitrary Inclined Leaves*) [58,59]. The latest recalibrated version PROSPECT-D [60,61] simulates bidirectional-hemispherical reflectance and transmittance in the optical domain as a function of leaf pigments (chlorophyll a+b content C_{ab}, carotenoids C_{ar}, and anthocyanins C_{anth}), dry matter C_m, and brown pigments C_{brown} as well as a leaf mesophyll structure parameter N, and EWT(C_w). The canopy model SAIL calculates a bidirectional reflectance factor of 1-D turbid medium plant canopies. With regard to leaf optical properties and reflectance of the underlying soil (p_{soil}), it implements canopy structure (LAI), average leaf inclination angle (ALA) or optionally, ellipsoidal leaf inclination distribution (LIDF), and hot spot size parameter (h_{spot}) for a given illumination and viewing geometry (observation zenith angle (OZA), relative azimuth angle (rAA) between sun and sensor, and the solar zenith angle (SZA)).

Considering the impact of plant foliar water on the 970 nm absorption band, during LUT generation, all parameters with sensitivity in the NIR region were uniformly distributed over a wide value range (Table 3). Leaf pigments, having no effect on reflectance in the NIR [26,44], remained constant.

Table 3. Parameter ranges for PROSPECT-D and PROSPECT-D + 4SAIL (PROSAIL) LUT. Specified ranges are uniformly distributed, single values are fixed.

PROSPECT-D-Parameters	Range	Notation [Unit]	4SAIL-Parameters	Range	Notation [Unit]
N	1.0–3.0	[-]	LAI	0.5–8.0	$[m^2\ m^{-2}]$
C_{ab}	55	$[\mu g\ cm^{-2}]$	ALA	0–90	[deg]
C_w	0.0002–0.07	$[g\ cm^{-2}]$	h_{spot}	0.01–0.5	[-]
C_m	0.001–0.02	$[g\ cm^{-2}]$	OZA	0	[deg]
C_{brown}	0.0–1.0	[-]	SZA	35–50	[deg]
C_{ar}	15	$[\mu g\ cm^{-2}]$	rAA	0	[deg]
C_{anth}	5	$[\mu g\ cm^{-2}]$	p_{soil}	0.0–1.0	[-]

3. Methods

3.1. The Beer-Lambert Law and Retrieval Method Development

The Beer-Lambert law is mathematically formulated as Equation (4):

$$\Phi = \Phi_0 e^{-\alpha(\lambda)d}. \tag{4}$$

Passing through a medium of thickness d the incident radiation intensity Φ_0 is exponentially attenuated with increasing penetration depth. The absorption characteristics of a medium are defined by its wavelength-dependent absorption coefficients $\alpha(\lambda)$. In this study, due to the accurate spectral resolution in the 970 nm domain [61], water absorption coefficients for pure liquid water as determined by Kou, et al. [11] are used. Furthermore, it is assumed that within the absorption band at 970 nm, water is the only quantity-depending, varying active absorber and that variance within absorption of further components is neglectable. Thus, concluding from Equation (4), the absorption depth of measured fresh leaves or canopies at 970 nm is uniquely dependent on the thickness of the optically active water layer (see also discussion in Section 3.2). For dry leaves or senescent canopies, absorption by liquid water is neglectable, resulting in a strictly linear reflectance signature at 970 nm. For the retrieval of EWT_{canopy}, Equation (4) is rearranged in accordance with Bach ([51]; Equation (5)), where R_0 is the measured reflectance, d is the thickness of the optically active water layer, and R' is the d-dependent reflectance:

$$R' = \frac{R_0}{e^{-\alpha(\lambda)d}} \tag{5}$$

Using Equation (5), d is iteratively optimized so that an objective function—the sum of absolute residuals between the modelled reflectance and the linear connection between the descending and ascending vertices of the 970 nm absorption—is minimal (Figure 2). The wavelength range considered by the plant water retrieval (PWR) model has been limited to 930–1060 nm based on preliminary minimization of the standard deviation of yielded EWT results from the PROSPECT LUT. Describing the thickness of the optically active water layer, the results can directly be compared to measured EWT on leaf level (Equation (1)), CWC (Equation (2)) and EWT_{canopy} (Equation (3)). The algorithm was implemented in Python, where retrieval of EWT for 50,000 spectra was completed in 69 s on an Intel Core i5-3570K @ 3.40 GHz.

3.2. Global Sensitivity Analysis

The PWR model expects the thickness of optically active water to reflect the vegetation water content detected by a hyperspectral sensor. Both the PROSPECT and PROSAIL LUT were subjected to a global sensitivity analysis (GSA) to identify and evaluate the impact of contributing parameters in the 970 nm domain and to validate the performance of the model. The Fourier amplitude sensitivity test (FAST) identifies the main effects (first-order sensitivity effects), i.e., the contribution (S_{Ti}) to the variance of the model output by each input variable and interactions with other variables [62]. The contribution of parameters to the 970 nm absorption depth and shape is assessed by its distribution width using the variance-to-mean ratio (VMR).
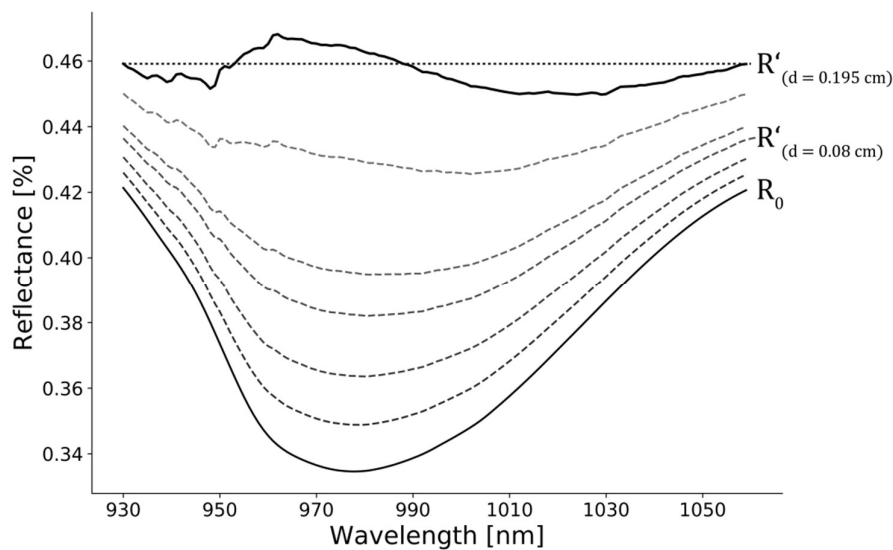
Figure 2. Determination of optically active water thickness *d* from a measured spectrum R_0 through minimization of residuals to assumed dry reflectance line (dotted line).

Within PROSPECT (Figure 3a) N contributes to 98% of leaf reflectance at the vertices left and right of the 970 nm water absorption band. At 970 nm C_w is the highest contributing parameter in terms of VMR (10^{-2}). Minor influence on the shape of the absorption band is caused by C_{brown} at the descending vertex (VMR = 10^{-3}). C_m and parameter interactions also affect overall reflectance at 970 nm but interference with its shape is smaller by more than two orders of magnitude (10^{-4}). Regarding PROSAIL (Figure 3b), C_w likewise is the strongest shape-determining factor at 970 nm in terms of VMR (10^{-2}). However, the 970 nm absorption shape is affected by canopy structural parameters (ALA, LAI, h_{spot}, p_{soil}) and parameter interactions. The sum of influential parameter VMR may exceed C_w VMR, which may result in masking of the water signal when unfavorable parameter combinations occur.
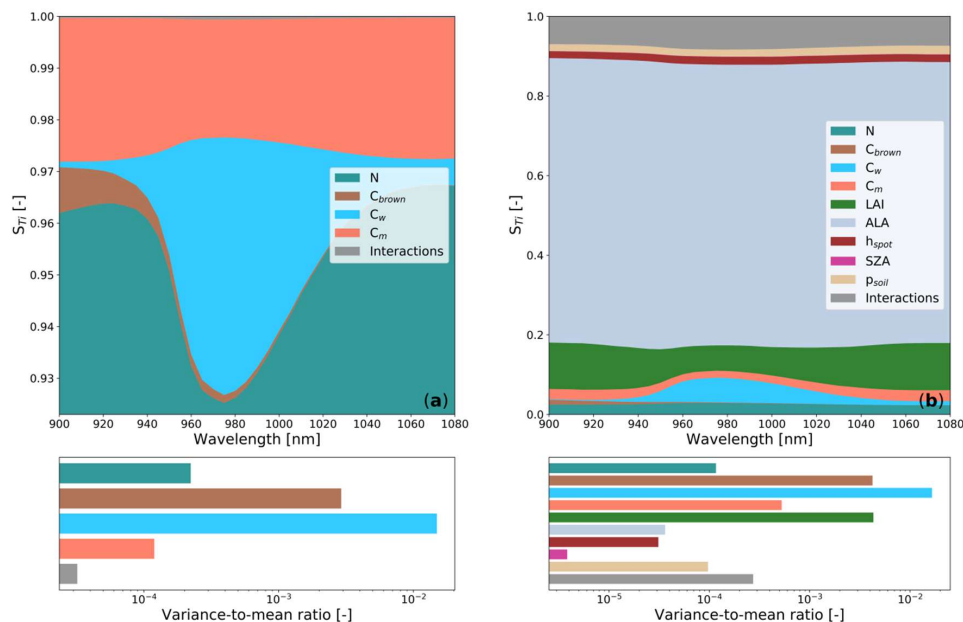
Figure 3. FAST first-order sensitivity coefficients and interactions (S_{Ti}) to reflectance (900–1080 nm) for PROSPECT (**a**) and PROSAIL (**b**) parameters. Due to high contribution of the leaf structure coefficient N within PROSPECT, only the upper contribution range ≥ 0.935 is shown. Below, influences of parameters that affect the shape of the water absorption band considered within the PWR model (930–1060 nm) are quantified by the variance-to-mean ratio (VMR).

The retrieval method was first tested on all the spectra within both the PROSPECT and the PROSAIL LUT (Figure 4). With a coefficient of determination (R^2) of 0.96 the approach indicates a strong correlation between PROSPECT modelled water content C_w and retrieved optically active water content EWT (Figure 4a). However, the high relative root mean square error ($rRMSE = RMSE * mean_{observations}^{-1}$) of 286% with an intercept close to zero revealed a strong systematical offset. The growing spread of results towards higher values of C_w suggests a simultaneously increasing influence of other parameters due to the exponential radiative transfer from specific absorption coefficients to transmission and reflectance [57].
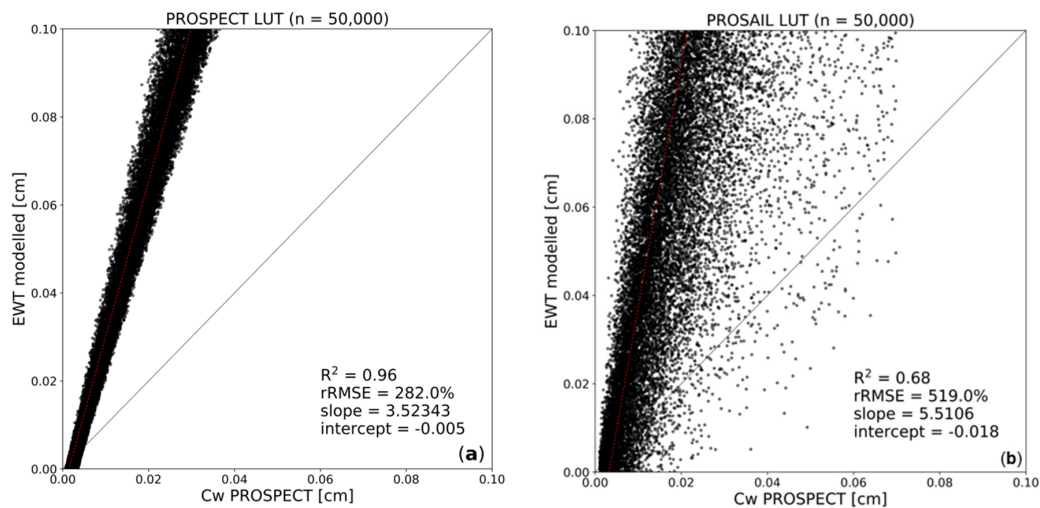
Figure 4. Modelled EWT results from synthetic LUT containing PROSPECT (**a**) and PROSAIL (**b**) spectra.

Applied to PROSAIL spectra (Figure 4b) the R^2-results (0.68) are significantly lower and although model results correspond to LUT C_w-values, both regression residuals and intercept do not show a systematic bias. However, within the created LUT, several parameter combinations can be considered unrealistic [63], masking or flattening the water signal due to model parameter related interference with the shape of the 970 nm absorption band. The resulting outliers and overall spread of modelled C_w-values render the PROSAIL LUT unsuitable for further calibration of the model.

*3.3. Using PROSPECT for Calibration of the PWR Model*

The model was further tested on the LOPEX93 [55] and ANGERS [56] datasets, which showed a similar systematical bias as model results from PROSPECT spectra (Figure 5a,c,e). Since the overestimation seemed to be solely defined by the slope of the regression line, the water absorption coefficients in Equation (5) were adjusted by multiplying the slope of the PROSPECT LUT linear regression model as a constant (Equation (6)):

$$R' = \frac{R_0}{e^{-\alpha(\lambda)d*3.52343}} \tag{6}$$

The calibration procedure accounts for unknown effects of the leaf surface and of leaf internal structure on reflectance in the 970 nm domain [61] and for potential multiple leaf internal scattering [44,64]. Using the calibrated water absorption coefficients (Equation (6)), minimization of the objective function is achieved more quickly, resulting in lower modelled values of EWT that are consistent with the measured order of magnitude. Subsequently, the altered absorption coefficients in the 930 to 1060 nm range were used for an improved water content retrieval. Applied to the PROSPECT LUT (Figure 5b), EWT was estimated with a much smaller error (rRMSE = 12%). Applying the

algorithm with updated coefficients to LOPEX93 data, measured EWT was estimated with $R^2 = 0.93$ and rRMSE = 22% and for ANGERS data with 0.93 and 39% respectively (Figure 5d,f).
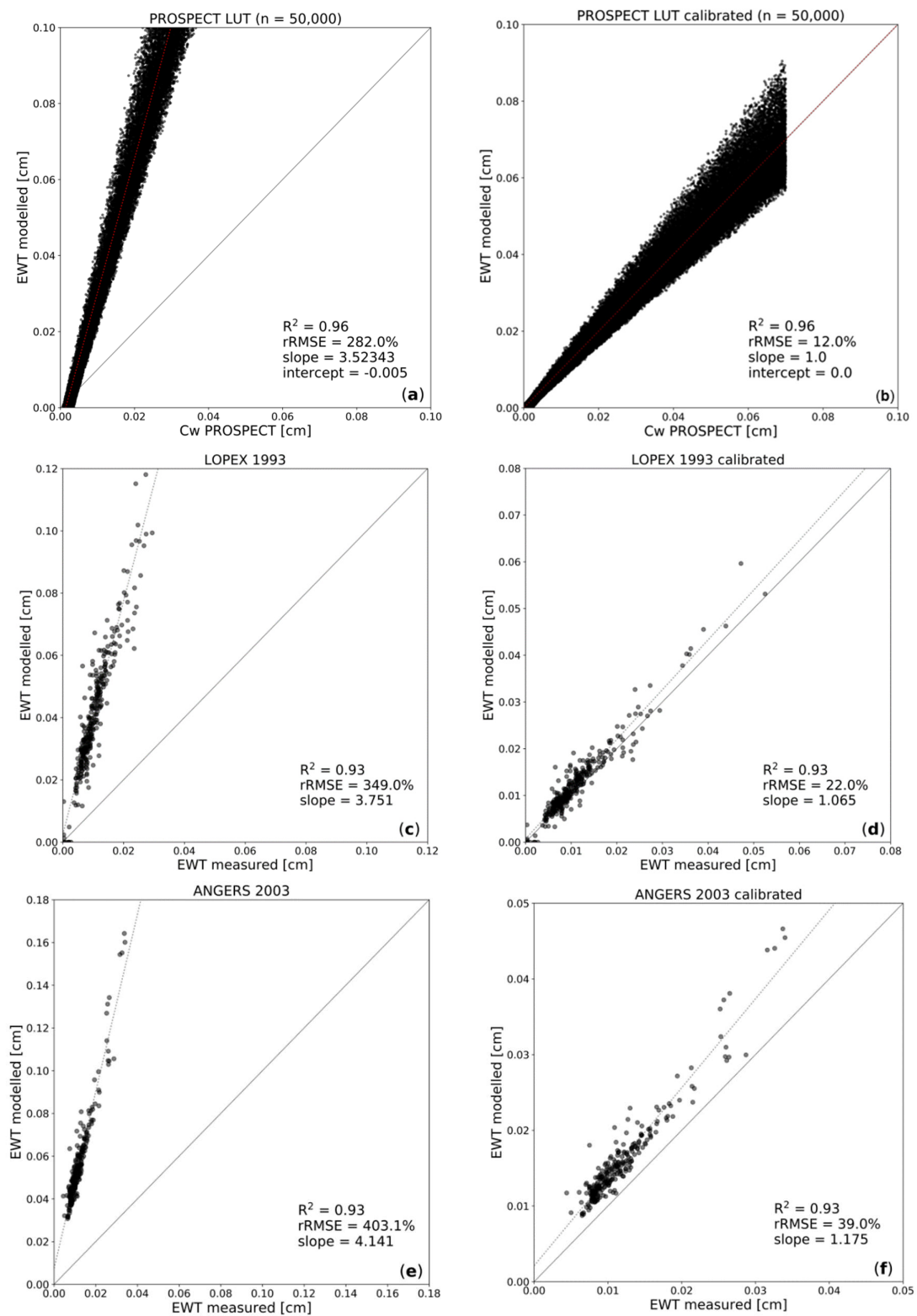

Figure 5. Uncalibrated PWR-results for the PROSPECT LUT (**a**); LOPEX93 data (**c**); and ANGERS data (**e**); compared to results after calibration: PROSPECT LUT (**b**) LOPEX93 (**d**); and ANGERS (**f**).

4. Results

The minimization process for retrieving optically active water using the PWR model with recalibrated absorption coefficients (factor 3.52342, Equation (6)) was applied to both in-situ winter wheat and corn spectral data. The results were compared to combinations of destructively measured leaf, stalk, and ear or cob water contents. For further analysis, the BBCH-scale was included to relate to growth stage dependencies of the model results.

4.1. Winter Wheat Data

Considering only the measured water content of wheat leaves, the results showed low correlation (Figure 6a: R^2 = 0.27; rRMSE = 81%); however, annotated BBCH-values showed good results for tillering (20+) and stalk elongation stages (30+) and progressing senescence (87). On the other hand, heading (47+) and flowering stages (60+) as well as ear development and ripening stages (70+) were invariably overestimated by the model. The sum of leaf and stalk water content yielded better results (Figure 6b: R^2 = 0.68; rRMSE = 52%) in particular for early growth stages. However, as growth proceeds, strong underestimation of EWT_{leaf} + EWT_{stalk} occurs due to saturation.
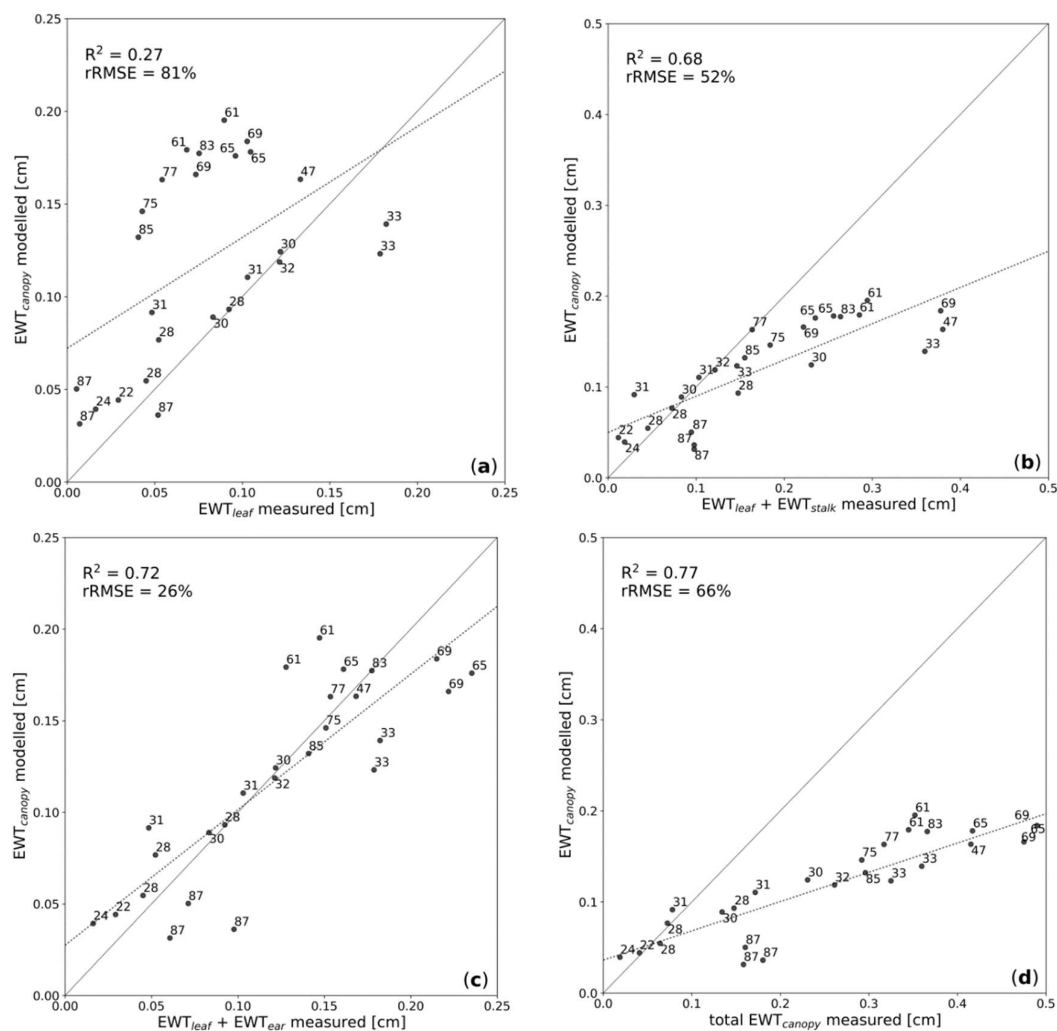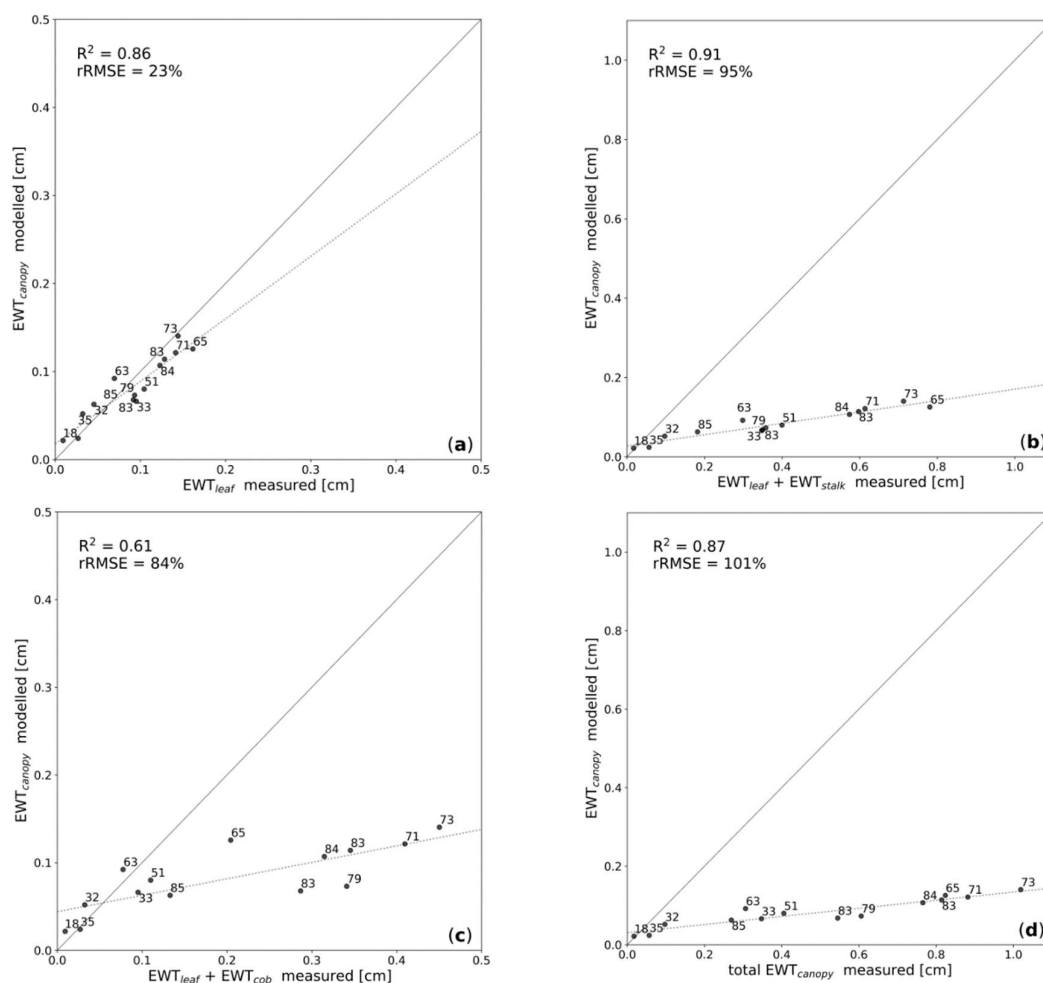

Figure 6. Modelled optically active water in relation to measured water contents of wheat compartments. Annotated numbers refer to secondary growth stages according to BBCH-scale. Results compared to EWT_{leaf} (**a**); EWT_{leaf} + EWT_{stalk} (**b**); EWT_{leaf} + EWT_{ear} (**c**); and total EWT_{canopy} (**d**).

The best results were obtained when combining the measured water contents of leaves and ears (Figure 6c: $R^2 = 0.72$; rRMSE = 26%). Thereby, model results adequately reflected measured $EWT_{leaf} + EWT_{ear}$ across all phenological stages over three years. Aggregating measured EWT_{leaf}, EWT_{stalk} and EWT_{ear} (= total EWT_{canopy}) yet again largely resulted in an underestimation (Figure 6d: $R^2 = 0.77$; rRMSE = 66%); only tillering stages were modelled with reasonable accuracy.

4.2. Corn Data

Regarding the two-year corn dataset, best results were achieved for leaf water contents (Figure 7a: $R^2 = 0.86$; rRMSE = 23%) with a minor tendency to underestimation towards higher growth stages. Despite good correlation, the combination of leaf and stalk measured water content was largely underestimated by the model (Figure 7b: $R^2 = 0.91$; rRMSE = 95%). Aggregated EWT_{leaf} and EWT_{cob} resulted in both lower correlation and error (Figure 7c: $R^2 = 0.61$; rRMSE = 84%) due to underestimation when cobs were registered.

Figure 7. Modelled optically active water in relation to measured water contents of corn compartments. Annotated numbers refer to secondary growth stages according to BBCH-scale. Results compared to EWT_{leaf} (**a**); $EWT_{leaf} + EWT_{stalk}$ (**b**); $EWT_{leaf} + EWT_{cob}$ (**c**); and total EWT_{canopy} (**d**).

In relation to total measured EWT_{canopy}, both correlation and underestimation are large (Figure 7d: $R^2 = 0.87$; rRMSE = 101%). In view of phenological dependencies, low water contents were consistently modelled with high accuracy during early leaf development stage (BBCH = 18) and beginning stalk elongation (30–32). Furthermore, unlike for wheat, no clear growth stage related dependencies were recognizable.

5. Discussion

5.1. Inversion of the Beer-Lambert Law for Water Content Retrieval

A simple physically based model was developed which applies the Beer-Lambert law to inversely retrieve optically active water content on leaf and canopy scale. In view of the fact that only one parameter—the thickness of the optically active water layer *d*—needs to be inverted, the algorithm allows a fast processing of large hyperspectral datasets. As shown by a GSA of the PROSPECT LUT in the 970 nm domain, interference of other parameters is marginal (Figure 3a) rendering C_w to be the dominant driver of leaf reflectance in this spectral region (R^2 = 0.96; Figure 4a). However, this does not apply to the PROSAIL LUT where, according to GSA, the cumulative influence of leaf and canopy structural parameters may mask the water signal (Figure 3b). Hereby, two issues interact: first, the 4SAIL model assumes a horizontally homogenous canopy, which may not be valid for complex canopy architectures and clumped vegetation through, e.g., formation in rows [65–67]. Second, unrealistic parameter combinations may occur in LUTs [63]. Both issues may unfavorably affect modelled reflectance in the 970 nm domain, reducing the predictive power of C_w for water content information (R^2 = 0.57; Figure 4b) and rendering the PROSAIL LUT unsuitable for calibration of the presented PWR model. When applied to PROSPECT spectra the linear offset of the regression model indicates that the absorption coefficients of pure liquid water differ from those of leaves, because reflectance in interaction with the leaf surface and multiple leaf internal reflections are not accounted for [44,64]. Using the slope of the regression from the PROSPECT LUT results as a factor to calibrate the absorption coefficients, the absolute quantification of PROSPECT C_w, LOPEX93 and ANGERS EWT significantly improved (Figure 5). The high correlation of R^2 = 0.96 between PROSPECT C_w and modelled EWT approved application of the model to in-situ measured TOC data. Nevertheless, using PROSPECT for calibration implies that potentially occurring canopy architectural effects on radiation [68] are being neglected. Hence, the PWR model considers the 970 nm absorption to be caused solely by liquid water. In addition, since reflected radiance in the 930–1060 nm range is also affected by atmospheric water vapor [16,46], the process of accurate atmospheric correction is a critical prerequisite when the PWR model is applied to future available hyperspectral TOC reflectance acquired from space.

5.2. Dependency of Canopy Water Detection on Canopy Structure

Absolute measures of EWT_{canopy} were inversely extracted from a three-year TOC winter wheat and two-year corn spectral dataset by means of the proposed PWR model. The results indicated a strong correlation between water absorption centered around 970 nm and measured EWT_{canopy}. However, the comparison of retrieved EWT_{canopy} from in-situ spectra with measured aggregations of plant compartment specific water contents raises the question, how deep radiation at 970 nm penetrates into the canopy and thus, which amounts of water actually can be observed by optical sensors [21]. Although absorption by water and vegetation in the NIR is low and penetration depth of radiation is higher in this wavelength range [6,69], the presented results showed that not all of the contained canopy water is detected by the sensor. Our results suggest that in the case of winter wheat modelled EWT_{canopy} largely reflects the absolute water contained in the leaves and present ears (Figure 6c). Taking only EWT_{leaf} as a reference, EWT_{canopy} is overestimated due to the presence of EWT_{ear}, which manifests in the spectral response but is not reflected by the in-situ data (Figure 6b,d). This also implies potential water content overestimation for wheat when referencing is done based on CWC records, which in the case of barley can be seen in the results of Vohland [3]. On the other hand, including measured EWT_{stalk}, the underestimation resulting with advanced growth stage indicates that radiation at 970 nm cannot penetrate increasingly hardened stalk tissue and thus cannot transport information about the water contained within. This has also been noted by Sims and Gamon [21] and Champagne, et al. [53]. This finding is further supported by the fact that residual water in ripe wheat (BBCH = 87) is consistently underestimated, rendering the PWR model unable to detect residual water in senescent wheat.

Despite good results of modelled EWT_{canopy} for EWT_{leaf} of corn, the results indicate a tendency to underestimation towards higher water contents (Figure 7a) due to maximum radiation transmission through stacked leaves [18]. Once stalks and cobs have developed, the underestimation of total corn EWT_{canopy} reveals the limited ability of NIR radiation to penetrate the thick stalk/cob tissues or the canopy depth or both (Figure 7b–d).

In summary, the retrieval results of winter wheat and corn vary because—depending on canopy structure—different plant components manifest in the 970 nm water absorption band. Several other studies also raised the fact of canopy structural influence on crop variables retrieval [68,70–73]. Cereal crops with prominent ears will not be satisfactorily modelled if the ear water content is not included in the in-situ measurements as it can be seen in the study of Champagne, et al. [53]. On the contrary, when modelling corn water content it may be sufficient to only collect leaf samples since only the water fraction of the leaves can be estimated directly from optical sensors. The specific structure of corn mostly covers the stalks and cobs, masking the water stored in these plant compartments.

In recent studies, mostly parametric regression models based on vegetation indices [3,49], derivative- [5,23], or integration-based [50] indices have been applied to retrieve crop canopy water content information from hyperspectral data. Verrelst, et al. [74] obtained very good CWC correlation on SPARC03 data ($R^2 = 0.95$) by applying Gaussian process regression with integrated sequential backward band removal. Cernicharo, et al. [24] used both an ANN and a LUT approach to estimate CWC from CHRIS/PROBA data ($R^2 = 0.82$ and $R^2 = 0.64$, respectively). Earlier studies which presented retrieval methods based on the Beer-Lambert law include Champagne, et al. [53] with good results for corn but an overestimation of wheat canopy water content, because EWT_{ear} has not been sampled separately (index of agreement $D = 0.80$ and $D = 0.38$, respectively). The findings of this study are also confirmed by the Beer-Lambert law based study of Sims and Gamon [21], in which best results for water content of thin tissues were obtained ($R^2 = 0.66$), whereas total canopy water content was underestimated ($R^2 = 0.35$).

The presented PWR model is considered superior to empirical regression models by its physical basis, allowing insights into the physical meaning of results, while outperforming other Beer-Lambert law based approaches by the possibility to infer absolute measures of canopy water content from measured TOC reflectance spectra. This absolute quantifiability of canopy water content represents a novelty among available retrieval approaches. Besides, the accurate underlying data basis proved transferability of the model to different sites and crop types and, given that a sensor detects the maximal depth of the 970 nm water absorption, promises applicability also to hyperspectral data on an operational basis.

6. Conclusions

The proposed PWR model based on the inversion of the Beer-Lambert law effectively succeeds in the determination of wheat EWT_{leaf} and EWT_{ear} with consistent results over a three-year dataset ($R^2 = 0.72$; $rRMSE = 26\%$). For corn EWT_{leaf} was estimated from two-year data with even better results ($R^2 = 0.86$; $rRMSE = 23\%$). Since the detectability of canopy water content fractions seems to be largely dependent on the crop type, its canopy structure, depth, and growth stage, it is recommended to collect EWT_{leaf}, EWT_{stalk} and EWT_{fruit} data and corresponding reflectance for different crop types over all phenological stages along the growing cycle. However, an evaluation is needed to assess limits of canopy water content retrieval in terms of optical radiation penetration depth through thick canopies and tissues, also in view of a possibly improved retrieval from off-nadir spectroscopy [75]. Our study could proof the transferability of the developed PWR model to other sites and crop types and represents a novelty in crop water content absolute quantifiability. The PWR model will be provided as a slim and applicable tool within the open source software EnMAP-Box [76] to accurately and efficiently retrieve water content information from ground-based, airborne and spaceborne hyperspectral data, as it will become available through future missions.

References

1. Running, S.W.; Gower, S. Forest-BGC, a general model of forest ecosystem processes for regional applications. Ii. Dynamic carbon allocation and nitrogen budgets. *Tree Physiol.* **1991**, *9*, 147–160. [CrossRef] [PubMed]

2. Running, S.W.; Nemani, R.R. Regional hydrologic and carbon balance responses of forests resulting from potential climate change. *Clim. Chang.* **1991**, *19*, 349–368. [CrossRef]

3. Vohland, M. Using imaging and non-imaging spectroradiometer data for the remote detection of vegetation water content. *J. Appl. Remote Sens.* **2008**, *2*, 023520. [CrossRef]

4. Hank, T.; Bach, H.; Mauser, W. Using a remote sensing-supported hydro-agroecological model for field-scale simulation of heterogeneous crop growth and yield: Application for wheat in central Europe. *Remote Sens.* **2015**, *7*, 3934–3965. [CrossRef]

5. Clevers, J.G.P.W.; Kooistra, L.; Schaepman, M.E. Estimating canopy water content using hyperspectral remote sensing data. *Int. J. Appl. Earth Obs. Geoinf.* **2010**, *12*, 119–125. [CrossRef]

6. Peñuelas, J.; Filella, I.; Biel, C.; Serrano, L.; Savé, R. The reflectance at the 950–970 nm region as an indicator of plant water status. *Int. J. Remote Sens.* **1993**, *14*, 1887–1905. [CrossRef]

7. Peñuelas, J.; Pinol, J.; Ogaya, R.; Filella, I. Estimation of plant water concentration by the reflectance water index wi (r900/r970). *Int. J. Remote Sens.* **1997**, *18*, 2869–2875. [CrossRef]

8. Hank, T.B.; Berger, K.; Bach, H.; Clevers, J.G.P.W.; Gitelson, A.; Zarco-Tejada, P.; Mauser, W. Spaceborne imaging spectroscopy for sustainable agriculture: Contributions and challenges. *Surv. Geophys.* **2018**. [CrossRef]

9. Tucker, C.J. Remote sensing of leaf water content in the near infrared. *Remote Sens. Environ.* **1980**, *10*, 23–32. [CrossRef]

10. Danson, F.M.; Steven, M.D.; Malthus, T.J.; Clark, J.A. High-spectral resolution data for determining leaf water content. *Int. J. Remote Sens.* **1992**, *13*, 461–470. [CrossRef]

11. Kou, L.; Labrie, D.; Chylek, P. Refractive indices of water and ice in the 0.65- to 2.5-μm spectral range. *Appl. Opt.* **1993**, *32*, 3531–3540. [CrossRef] [PubMed]

12. Hardisky, M.; Klemas, V.; Smart, R.M. The influence of soil salinity, growth form, and leaf moisture on the spectral radiance of spartina alterniflora canopies. *Photogramm. Eng. Remote Sens.* **1983**, *49*, 77–83.

13. Hunt, E.R.; Rock, B.N.; Nobel, P.S. Measurement of leaf relative water content by infrared reflectance. *Remote Sens. Environ.* **1987**, *22*, 429–435. [CrossRef]

14. Hunt, E.R.; Rock, B.N. Detection of changes in leaf water content using near- and middle-infrared reflectances. *Remote Sens. Environ.* **1989**, *30*, 43–54.

15. Gao, B.-C. NDWI—A normalized difference water index for remote sensing of vegetation liquid water from space. *Remote Sens. Environ.* **1996**, *58*, 257–266. [CrossRef]

16. Datt, B. Remote sensing of water content in eucalyptus leaves. *Aust. J. Bot.* **1999**, *47*, 909–923. [CrossRef]

17. Jacquemoud, S.; Verhoef, W.; Baret, F.; Bacour, C.; Zarco-Tejada, P.J.; Asner, G.P.; François, C.; Ustin, S.L. Prospect+SAIL models: A review of use for vegetation characterization. *Remote Sens. Environ.* **2009**, *113*, S56–S66. [CrossRef]

18. Lillesaeter, O. Spectral reflectance of partly transmitting leaves: Laboratory measurements and mathematical modeling. *Remote Sens. Environ.* **1982**, *12*, 247–254. [CrossRef]

19. Newton, J.E.; Blackman, G.E. The penetration of solar radiation through leaf canopies of different structure. *Ann. Bot.* **1970**, *34*, 329–348. [CrossRef]

20. Bull, C.R. Wavelength selection for near-infrared reflectance moisture meters. *J. Agric. Eng. Res.* **1991**, *49*, 113–125. [CrossRef]

21. Sims, D.A.; Gamon, J.A. Estimation of vegetation water content and photosynthetic tissue area from spectral reflectance: A comparison of indices based on liquid water and chlorophyll absorption features. *Remote Sens. Environ.* **2003**, *84*, 526–537. [CrossRef]

22. Ghulam, A.; Li, Z.-L.; Qin, Q.; Yimit, H.; Wang, J. Estimating crop water stress with ETM+ NIR and SWIR data. *Agric. For. Meteorol.* **2008**, *148*, 1679–1695. [CrossRef]

23. Clevers, J.G.P.W.; Kooistra, L.; Schaepman, M.E. Using spectral information from the NIR water absorption features for the retrieval of canopy water content. *Int. J. Appl. Earth Obs. Geoinf.* **2008**, *10*, 388–397. [CrossRef]

24. Cernicharo, J.; Verger, A.; Camacho, F. Empirical and physical estimation of canopy water content from CHRIS/PROBA data. *Remote Sens.* **2013**, *5*, 5265. [CrossRef]

25. Verrelst, J.; Camps-Valls, G.; Muñoz-Marí, J.; Rivera, J.P.; Veroustraete, F.; Clevers, J.G.P.W.; Moreno, J. Optical remote sensing and the retrieval of terrestrial vegetation bio-geophysical properties—A review. *ISPRS J. Photogramm. Remote Sens.* **2015**, *108*, 273–290. [CrossRef]

26. Ceccato, P.; Flasse, S.; Tarantola, S.; Jacquemoud, S.; Grégoire, J.-M. Detecting vegetation leaf water content using reflectance in the optical domain. *Remote Sens. Environ.* **2001**, *77*, 22–33. [CrossRef]

27. Zarco-Tejada, P.J.; Rueda, C.A.; Ustin, S.L. Water content estimation in vegetation with MODIS reflectance data and model inversion methods. *Remote Sens. Environ.* **2003**, *85*, 109–124. [CrossRef]

28. Yilmaz, M.T.; Hunt, E.R.; Jackson, T.J. Remote sensing of vegetation water content from equivalent water thickness using satellite imagery. *Remote Sens. Environ.* **2008**, *112*, 2514–2522. [CrossRef]

29. Baret, F.; Guyot, G. Potentials and limits of vegetation indices for LAI and APAR assessment. *Remote Sens. Environ.* **1991**, *35*, 161–173. [CrossRef]

30. Houborg, R.; Soegaard, H.; Boegh, E. Combining vegetation index and model inversion methods for the extraction of key vegetation biophysical parameters using terra and aqua MODIS reflectance data. *Remote Sens. Environ.* **2007**, *106*, 39–58. [CrossRef]

31. Verrelst, J.; Malenovský, Z.; Van der Tol, C.; Camps-Valls, G.; Gastellu-Etchegorry, J.-P.; Lewis, P.; North, P.; Moreno, J. Quantifying vegetation biophysical variables from imaging spectroscopy data: A review on retrieval methods. *Surv. Geophys.* **2018**. [CrossRef]

32. Jacquemoud, S.; Bacour, C.; Poilvé, H.; Frangi, J.P. Comparison of four radiative transfer models to simulate plant canopies reflectance: Direct and inverse mode. *Remote Sens. Environ.* **2000**, *74*, 471–481. [CrossRef]

33. Atzberger, C.; Richter, K. Spatially constrained inversion of radiative transfer models for improved LAI mapping from future sentinel-2 imagery. *Remote Sens. Environ.* **2012**, *120*, 208–218. [CrossRef]

34. Labate, D.; Ceccherini, M.; Cisbani, A.; De Cosmo, V.; Galeazzi, C.; Giunti, L.; Melozzi, M.; Pieraccini, S.; Stagi, M. The PRISMA payload optomechanical design, a high performance instrument for a new hyperspectral mission. *Acta Astronaut.* **2009**, *65*, 1429–1436. [CrossRef]

35. Lee, C.M.; Cable, M.L.; Hook, S.J.; Green, R.O.; Ustin, S.L.; Mandl, D.J.; Middleton, E.M. An introduction to the NASA hyperspectral InfraRed imager (HyspIRI) mission and preparatory activities. *Remote Sens. Environ.* **2015**, *167*, 6–19. [CrossRef]

36. Feingersh, T.; Eyal, B.D. SHALOM—A commercial hyperspectral space mission. In *Optical Payloads for Space Missions*; Qian, S.-E., Ed.; John Wiley & Sons: Hoboken, NJ, USA, 2015.

37. Nieke, J.; Rast, M. Towards the copernicus hyperspectral imaging mission for the environment (CHIME). In Proceedings of the IGGARS 2018, Valencia, Spain, 22–27 July 2018; pp. 157–159.

38. Guanter, L.; Kaufmann, H.; Segl, K.; Foerster, S.; Rogass, C.; Chabrillat, S.; Kuester, T.; Hollstein, A.; Rossner, G.; Chlebek, C.; et al. The enmap spaceborne imaging spectroscopy mission for earth observation. *Remote Sens.* **2015**, *7*, 8830–8857. [CrossRef]

39. Green, R.O.; Conel, J.E.; Margolis, J.; Bruegge, J.C.; Hoover, L.G. An inversion algorithm for retrieval of atmospheric and leaf water absorption from AVIRIS radiance with compensation for atmospheric scattering. In *Third Airborne Visible/Infrared Imaging Spectrometer (AVIRIS) Workshop*; Green, O.R., Ed.; NASA: Pasadena, CA, USA, 1991; pp. 51–61.

40. Green, R.O.; Conel, J.E.; Roberts, D.A. Estimation of aerosol optical depth, pressure elevation, water vapor, and calculation of apparent surface reflectance from radiance measured by the airborne visible/infrared imaging spectrometer (AVIRIS). In Proceedings of the Summaries of the 4th Annual JPL Airborne Geoscience Workshop, AVJRIS Workshop, Washington, DC, USA, 25–29 October 1993; Volume 1937, pp. 73–76.

41. Ustin, S.L.; Riaño, D.; Hunt, E.R. Estimating canopy water content from spectroscopy. *Isr. J. Plant Sci.* **2012**, *60*, 9–23. [CrossRef]

42. Hunt, E.R.; Ustin, S.L.; Riaño, D. Remote sensing of leaf, canopy, and vegetation water contents for satellite environmental data records. In *Satellite-Based Applications on Climate Change*; Qu, J., Powell, A., Sivakumar, M.V.K., Eds.; Springer: Dordrecht, The Netherlands, 2013; pp. 335–357.

43. Knipling, E.B. Physical and physiological basis for the reflectance of visible and near-infrared radiation from vegetation. *Remote Sens. Environ.* **1970**, *1*, 155–159. [CrossRef]

44. Carter, G.A. Primary and secondary effects of water content on the spectral reflectance of leaves. *Am. J. Bot.* **1991**, *78*, 916–924. [CrossRef]

45. Gao, B.-C.; Goetz, A.F.H. Column atmospheric water vapor and vegetation liquid water retrievals from airborne imaging spectrometer data. *J. Geophys. Res. Atmos.* **1990**, *95*, 3549–3564. [CrossRef]

46. Gao, B.-C.; Goetz, A.F.H. Retrieval of equivalent water thickness and information related to biochemical components of vegetation canopies from AVIRIS data. *Remote Sens. Environ.* **1995**, *52*, 155–162. [CrossRef]

47. Green, R.O.; Painter, T.H.; Roberts, D.A.; Dozier, J. Measuring the expressed abundance of the three phases of water with an imaging spectrometer over melting snow. *Water Resour. Res.* **2006**, *42*. [CrossRef]

48. Thompson, D.R.; Gao, B.-C.; Green, R.O.; Roberts, D.A.; Dennison, P.E.; Lundeen, S.R. Atmospheric correction for global mapping spectroscopy: ATREM advances for the HyspIRI preparatory campaign. *Remote Sens. Environ.* **2015**, *167*, 64–77. [CrossRef]

49. Yi, Q.; Wang, F.; Bao, A.; Jiapaer, G. Leaf and canopy water content estimation in cotton using hyperspectral indices and radiative transfer models. *Int. J. Appl. Earth Obs. Geoinf.* **2014**, *33*, 67–75. [CrossRef]

50. Pasqualotto, N.; Delegido, J.; Van Wittenberghe, S.; Verrelst, J.; Rivera, J.P.; Moreno, J. Retrieval of canopy water content of different crop types with two new hyperspectral indices: Water absorption area index and depth water index. *Int. J. Appl. Earth Obs. Geoinf.* **2018**, *67*, 69–78. [CrossRef]

51. Bach, H. *Die Bestimmung Hydrologischer und Landwirtschaftlicher Oberflächenparameter aus Hyperspektralen Fernerkundungsdaten*; Geobuch-Verlag: München, Germany, 1995.

52. Ustin, S.L.; Roberts, D.A.; Pinzón, J.; Jacquemoud, S.; Gardner, M.; Scheer, G.; Castañeda, C.M.; Palacios-Orueta, A. Estimating canopy water content of chaparral shrubs using optical methods. *Remote Sens. Environ.* **1998**, *65*, 280–291. [CrossRef]

53. Champagne, C.M.; Staenz, K.; Bannari, A.; McNairn, H.; Deguise, J.-C. Validation of a hyperspectral curve-fitting model for the estimation of plant water content of agricultural canopies. *Remote Sens. Environ.* **2003**, *87*, 148–160. [CrossRef]

54. Meier, U. *Growth Stages of Mono- and Dicotyledonous Plants: BBCH Monograph*; Open Agrar Repositorium: Quedlinburg, Germany, 2018.

55. Hosgood, B.; Jacquemoud, S.; Andreoli, J.; Verdebout, A.; Pedrini, A.; Schmuck, G. *Leaf Optical Properties Experiment 93 (LOPEX93)*; European Commission: Brussels, Belgium, 1995.

56. Jacquemoud, S.; Bidel, C.; Pavan, F.G. Angers Leaf Optical Properties Database. 2003. Available online: http://ecosis.org (accessed on 14 November 2017).

57. Jacquemoud, S.; Baret, F. Prospect: A model of leaf optical properties spectra. *Remote Sens. Environ.* **1990**, *34*, 75–91. [CrossRef]

58. Verhoef, W. Light scattering by leaf layers with application to canopy reflectance modeling: The sail model. *Remote Sens. Environ.* **1984**, *16*, 125–141. [CrossRef]

59. Verhoef, W.; Bach, H. Coupled soil–leaf-canopy and atmosphere radiative transfer modeling to simulate hyperspectral multi-angular surface reflectance and TOA radiance data. *Remote Sens. Environ.* **2007**, *109*, 166–182. [CrossRef]

60. Féret, J.B.; Gitelson, A.A.; Noble, S.D.; Jacquemoud, S. Prospect-D: Towards modeling leaf optical properties through a complete lifecycle. *Remote Sens. Environ.* **2017**, *193*, 204–215. [CrossRef]

61. Feret, J.-B.; François, C.; Asner, G.P.; Gitelson, A.A.; Martin, R.E.; Bidel, L.P.R.; Ustin, S.L.; le Maire, G.; Jacquemoud, S. Prospect-4 and 5: Advances in the leaf optical properties model separating photosynthetic pigments. *Remote Sens. Environ.* **2008**, *112*, 3030–3043. [CrossRef]

62. Cannavó, F. Sensitivity analysis for volcanic source modeling quality assessment and model selection. *Comput. Geosci.* **2012**, *44*, 52–59. [CrossRef]

63. Wang, Z.; Skidmore, A.K.; Darvishzadeh, R.; Wang, T. Mapping forest canopy nitrogen content by inversion of coupled leaf-canopy radiative transfer models from airborne hyperspectral imagery. *Agric. For. Meteorol.* **2018**, *253–254*, 247–260. [CrossRef]

64. Zhang, Q.; Li, Q.; Zhang, G. Scattering impact analysis and correction for leaf biochemical parameter estimation using vis-NIR spectroscopy. *Spectroscopy* **2011**, *26*, 28–39.

65. Dorigo, W.A. Improving the robustness of cotton status characterisation by radiative transfer model inversion of multi-angular CHRIS/PROBA data. *IEEE J. Sel. Top. Appl. Earth Obs. Remote Sens.* **2012**, *5*, 18–29. [CrossRef]

66. Zou, X.; Hernandez Clemente, R.; Tammeorg, P.; Lizarazo, C.; Stoddard, F.; Mäkelä, P.; Pellikka, P.; Mõttus, M. Retrieval of leaf chlorophyll content in field crops using narrow-band indices: Effects of leaf area index and leaf mean tilt angle. *Int. J. Remote Sens.* **2015**, *36*, 6031–6055. [CrossRef]

67. Combal, B.; Baret, F.; Weiss, M.; Trubuil, A.; Macé, D.; Pragnère, A.; Myneni, R.; Knyazikhin, Y.; Wang, L. Retrieval of canopy biophysical variables from bidirectional reflectance: Using prior information to solve the ill-posed inverse problem. *Remote Sens. Environ.* **2003**, *84*, 1–15. [CrossRef]

68. Kuester, T.; Spengler, D. Structural and spectral analysis of cereal canopy reflectance and reflectance anisotropy. *Remote Sens.* **2018**, *10*, 1767. [CrossRef]

69. Serrano, L.; Ustin, S.L.; Roberts, D.A.; Gamon, J.A.; Peñuelas, J. Deriving water content of chaparral vegetation from AVIRIS data. *Remote Sens. Environ.* **2000**, *74*, 570–581. [CrossRef]

70. Trombetti, M.; Riaño, D.; Rubio, M.A.; Cheng, Y.B.; Ustin, S.L. Multi-temporal vegetation canopy water content retrieval and interpretation using artificial neural networks for the continental USA. *Remote Sens. Environ.* **2008**, *112*, 203–215. [CrossRef]

71. Berger, K.; Hank, T.; Vuolo, F.; Mauser, W.; D'Urso, G. Optimal exploitation of the sentinel-2 spectral capabilities for crop leaf area index mapping. *Remote Sens.* **2012**, *4*, 561–582.

72. Richter, K.; Hank, T.B.; Mauser, W.; Atzberger, C. Derivation of biophysical variables from earth observation data: Validation and statistical measures. *J. Appl. Remote Sens.* **2012**, *6*, 063557. [CrossRef]

73. Transon, J.; d'Andrimont, R.; Maugnard, A.; Defourny, P. Survey of hyperspectral earth observation applications from space in the sentinel-2 context. *Remote Sens.* **2018**, *10*, 157. [CrossRef]

74. Verrelst, J.; Rivera, J.P.; Gitelson, A.; Delegido, J.; Moreno, J.; Camps-Valls, G. Spectral band selection for vegetation properties retrieval using Gaussian processes regression. *Int. J. Appl. Earth Obs. Geoinf.* **2016**, *52*, 554–567. [CrossRef]

75. Danner, M.; Berger, K.; Wocher, M.; Mauser, W.; Hank, T. Retrieval of biophysical crop variables from multi-angular canopy spectroscopy. *Remote Sens.* **2017**, *9*, 726. [CrossRef]

76. van der Linden, S.; Rabe, A.; Held, M.; Jakimow, B.; Leitão, P.; Okujeni, A.; Schwieder, M.; Suess, S.; Hostert, P. The EnMAP-Box—A toolbox and application programming interface for EnMAP data processing. *Remote Sens.* **2015**, *7*, 11249. [CrossRef]